

# Regularization of Inverse Problems via Time Discrete Geodesics in Image Spaces

Sebastian Neumayer\*    Johannes Persch\*    Gabriele Steidl\*<sup>†</sup>

September 1, 2022

This paper addresses the solution of inverse problems in imaging given an additional reference image. We combine a modification of the discrete geodesic path model of Berkels, Effland and Rumpf with a variational model, actually the  $L^2$ - $TV$  model, for image restoration. We prove that the space continuous model has a minimizer and propose a minimization procedure which alternates over the involved sequences of deformations and images. The minimization with respect to the image sequence exploits recent algorithms from convex analysis to minimize the  $L^2$ - $TV$  functional. For the numerical computation we apply a finite difference approach on staggered grids together with a multilevel strategy. We present proof-of-the-concept numerical results for sparse and limited angle computerized tomography as well as for superresolution demonstrating the power of the method.

## 1. Introduction

In certain applications it makes sense to account for qualitative prior image information to improve the image reconstruction. Typical examples are tomographic imaging problems with sparsely or limited angle sampled sinogram data. One possibility to incorporate a reference image into the reconstruction process is to take its deformation towards the image of interest, which is only indirectly given by measurements, into account. Recent work in this direction show promising results. Schumacher, Modersitzki and Fischer [42] have dealt with the combined reconstruction and motion correction in SPECT imaging. Karlsson and Ringh [25] coupled the optimal transport model with inverse problems. Chen and Öktem [14] tackled hard inverse problems with shape priors under the name *indirect image registration* within the large deformation diffeomorphic metric mapping (LDDMM) framework and in an earlier paper [34] via linearized deformations. The authors use ODE constrained problem formulations, where the regularizing of the deformations exploits reproducing kernel Hilbert spaces. As a drawback, the LDDMM

---

<sup>†</sup>Department of Mathematics, Technische Universität Kaiserslautern, Paul-Ehrlich-Str. 31, D-67663 Kaiserslautern, Germany, {sneumaye,persch,steidl}@mathematik.uni-kl.de.

<sup>2</sup>Fraunhofer ITWM, Fraunhofer-Platz 1, D-67663 Kaiserslautern, Germany

[6, 15, 17, 43, 44] based methods can only deal with images having the same intensities. The metamorphosis model of Miller, Trounev and Younes [29, 45, 46] is an extension of the LDDMM approach which allows the variation of the image intensities along trajectories of the pixels. A comprehensive overview over the topic is given in the book [50] as well as in the review article [28]. For a historic account see also [27]. In a recent preprint, Gris and Öktem [21] have enlarged the ideas in [14, 34] to the metamorphosis setting.

In our paper, we also follow the metamorphosis idea, but in a completely different way than in [21]. We built up on the time discrete geodesic calculus proposed for shape spaces by Rumpf and Wirth [39, 40] and for images by Berkels, Rumpf and Effland [7]. For convergence of the time discrete path model to the metamorphosis one we refer to these papers. Here deformations are modeled via a smoothness term and the linearized elastic potential, which is also a usual choice in registration problems. We combine this model with a „usual“ variational image reconstruction model, actually the  $L^2$ - $TV$  model, which originated from [38]. Then we can merge recent primal-dual minimization algorithms from convex analysis with a Quasi-Newton approach from image registration.

Let  $\mathcal{X}, \mathcal{Y}$  be Hilbert spaces and  $A \in L(\mathcal{X}, \mathcal{Y})$  a linear, continuous operator. A typical space  $\mathcal{X}$  will be the space of square integrable function  $L^2(\Omega)$  defined over some image domain  $\Omega \subset \mathbb{R}^2$ . We want to reconstruct an unknown image  $I_{\text{orig}} \in \mathcal{X}$  having the following information available:

- I1) an image  $B = AI_{\text{orig}} + \eta \in \mathcal{Y}$ , where  $\eta$  denotes some small error, e.g. due to noise.
- I2) a reference image  $R$  which is similar to the original image.

A usual variational model to approximate  $I_{\text{orig}}$  from  $B$  using only I1) is given by

$$\arg \min_{I \in \mathcal{X}} \mathcal{E}(I; B) := \mathcal{D}(I; B) + \alpha \mathcal{P}(I), \quad \alpha \geq 0, \quad (1)$$

where  $\mathcal{D}$  is a data term and  $\mathcal{P}$  a prior or regularizer. A model for edge-preserving image restoration is the  $L^2$ - $TV$  model, which will be also our model of choice.

To incorporate the reference image  $R$ , we want to combine model (1) with a modified version of the time discrete geodesic model of Berkels, Effland and Rumpf [7]. Given a template image  $I_0 = T$  and a reference image  $I_K = R$ , this model aims to find a chain of smooth deformations  $(\varphi_0, \dots, \varphi_{K-1})$  from an appropriately defined admissible set  $\mathcal{A}$  together with a sequence of images  $(I_1, \dots, I_{K-1})$  such that the sum of the quadratic distances

$$\sum_{k=0}^{K-1} \|I_k \circ \varphi_k^{-1} - I_{k+1}\|_{\mathcal{X}}^2 \quad (2)$$

together with a prior

$$\sum_{k=0}^{K-1} \int_{\Omega} \nu |D^m \varphi_k|^2 + W(D\varphi_k) dx, \quad \nu > 0$$

on the deformations becomes small, see Fig. 1. The first part of the deformation regularization enforces the smoothness of the mappings, while the second term, circumscribed by  $W$ , will be chosen as linearized elastic potential. By (2), the image sequence  $(T, I_1, \dots, R)$  may differ from the deformed image sequence  $(T, T \circ \varphi_0^{-1}, \dots, T \circ \varphi_0^{-1} \circ \dots \circ \varphi_{K-1}^{-1})$ , which makes the model flexible for intensity changes.

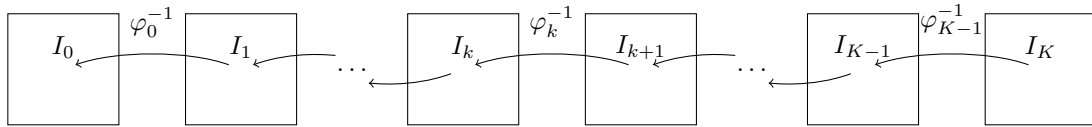


Figure 1: Illustration of the image and diffeomorphism path, where  $I_{k+1}(x) \approx I_k(\varphi_k^{-1}(x))$ ,  $k = 0, \dots, K - 1$ .

**Outline of the Paper** In Section 2, we introduce the necessary preliminaries concerning the spaces of deformations and images. In particular, we highlight properties of the concatenations of admissible deformations and  $L^2$  images. This motivates the modification of the time discrete path model [7] and also of our generalized model for manifold-valued images in [32]. In Section 3, we establish our space continuous restoration model. Since it combines time discrete morphing with inverse problems we call it TDM-INV model. We prove that it has a minimizer. Section 4 deals with a minimization procedure. For minimizing the image sequence we incorporate primal-dual algorithms from convex analysis. Further, we explain computational issues in the space discrete setting. The numerical examples in Section 5 demonstrate the very good performance of our algorithm. We finish with conclusions in Section 6.

## 2. Preliminaries

In the rest of this paper, let  $\Omega \subset \mathbb{R}^n$  be a nonempty open connected bounded set with Lipschitz boundary. In this section, we introduce admissible sets  $\mathcal{A}$  of deformations and consider the concatenations of such mappings with images from  $L^2(\Omega)$ . We will see that  $I \circ \varphi$  considered in [7] is in general not in  $L^2(\Omega)$  while  $I \circ \varphi^{-1} \in L^2(\Omega)$ . Therefore we prefer to modify the time discrete geodesic path model by using use the later concatenation. Note that the image space  $L^\infty$  was treated in [18], while we have used a restricted admissible set for the diffeomorphisms in [32].

### 2.1. Admissible Deformations

First, we introduce the smoothness spaces of our deformation mappings. Let  $C^{k,\alpha}(\bar{\Omega})$ ,  $k \in \mathbb{N}_0$ , denote the Hölder space of functions  $f \in C^k(\bar{\Omega})$  for which

$$\|f\|_{C^{k,\alpha}(\bar{\Omega})} := \sum_{|\beta| \leq k} \|D^\beta f\|_{C(\bar{\Omega})} + \sum_{|\beta|=k} \sup_{\substack{x,y \in \Omega \\ x \neq y}} \frac{|D^\beta f(x) - D^\beta f(y)|}{|x - y|^\alpha}$$

is finite. With this norm  $C^{k,\alpha}(\bar{\Omega})$  is a Banach space.

By  $W^{m,p}(\Omega)$ ,  $m \in \mathbb{N}$ ,  $1 \leq p < \infty$ , we denote the Sobolev space of functions having weak derivatives up to order  $m$  in  $L^p(\Omega)$  with norm

$$\|f\|_{W^{m,p}(\Omega)}^p := \int_{\Omega} \sum_{|\alpha| \leq m} |D^\alpha f(x)|^p dx.$$

We apply the usual abbreviation  $|D^m f|^p := \sum_{|\alpha|=m} |D^\alpha f|^p$ . For  $F = (f_\nu)_{\nu=1}^n$ , we set  $|D^m F|^p = \sum_{\nu=1}^n |D^m f_\nu|^p$ . In particular, we are interested in  $W^{m,2}(\Omega)$  with  $m > 1 + \frac{n}{2}$ . In this case,  $W^{m,2}(\Omega)$  is compactly embedded in  $C^{1,\alpha}(\bar{\Omega})$  for all  $\alpha \in (0, m - 1 - \frac{n}{2})$  [1, p. 350, Th. 8.13] and consequently  $W^{m,2}(\Omega) \hookrightarrow W^{1,p}(\Omega)$  for all  $p \geq 1$ .

We assume that the mappings  $\varphi$  lie in the following admissible set

$$\mathcal{A} := \{\varphi \in (W^{m,2}(\Omega))^n : \det(D\varphi) > 0 \text{ a.e. in } \Omega, \varphi(x) = x \text{ for } x \in \partial\Omega\},$$

where  $m > 1 + \frac{n}{2}$ . Then  $\varphi$  has certain useful properties. By a result of Ball [3], we have

i)  $\varphi(\bar{\Omega}) = \bar{\Omega}$ .

ii)  $\varphi$  maps measurable sets in  $\bar{\Omega}$  to measurable sets in  $\bar{\Omega}$  and the change of variable formula

$$\int_B I(\varphi(x)) \det(D\varphi)(x) dx = \int_{\varphi(B)} I(y) dy$$

holds for any measurable set  $B \subset \bar{\Omega}$  and any measurable function  $I : \mathbb{R}^n \rightarrow \mathbb{R}$  provided that one of the above integrals exists.

iii)  $\varphi$  is injective a.e., i.e., the set

$$S := \{x \in \bar{\Omega} : \varphi^{-1}(x) \text{ has more than one element}\}$$

has Lebesgue measure zero.

By property i) and since  $\bar{\Omega}$  is bounded, it follows immediately for all  $\varphi \in \mathcal{A}$  that

$$\|\varphi\|_{(L^\infty(\Omega))^n} \leq C, \quad \|\varphi\|_{(L^2(\Omega))^n} \leq C, \quad (3)$$

with constants depending only on  $\Omega$ . By the embedding properties of Sobolev spaces we have  $\varphi \in (C^{1,\alpha}(\bar{\Omega}))^n$ . Further, by the inverse mapping theorem  $\varphi^{-1}$  exists locally around a.e.  $x \in \Omega$  and is continuously differentiable on the corresponding neighborhood. However, to guarantee that  $\varphi^{-1}$  is continuous (or, even more, continuously differentiable) further assumptions are required, see [3, Theorem 2]. Take for example the function  $\varphi(x) := x^3$  on  $\Omega := (-1, 1)$  which is in  $\mathcal{A}$  but  $\varphi^{-1} = \text{sgn}(x)|x|^{\frac{1}{3}}$  is not continuously differentiable.

## 2.2. Space of Images

In this paper, we consider images as functions in  $\mathcal{X} := L^2(\Omega)$ . Unfortunately, the concatenation of  $I \in L^2(\Omega)$  with  $\varphi \in \mathcal{A}$  can result in a function

$$I \circ \varphi \notin L^2(\Omega),$$

as the example  $I(x) := x^{-\frac{1}{4}}$  in  $L^2((0, 1))$  and  $\varphi(x) := x^2$  shows. However, we will see that

$$\varphi \circ I := I \circ \varphi^{-1} \in L^2(\Omega), \quad (4)$$

where we have to define the function properly. To this end, let  $\mathcal{N}$  be a Borel null set containing  $S$  from iii). Then  $\mathcal{B} := \Omega \setminus \mathcal{N}$  is a Borel set with  $\mu(\mathcal{B}) = \mu(\Omega)$ . Note that  $\varphi^{-1}(\mathcal{B})$  is itself a Borel set since  $\varphi \in (W^{m,2}(\Omega))^n$  is measurable. Consider  $\varphi^{-1} : \mathcal{B} \rightarrow \varphi^{-1}(\mathcal{B})$  and let  $B \subseteq \varphi^{-1}(\mathcal{B})$  be a Borel set. Then, by ii), we see that  $(\varphi^{-1})^{-1}(B) = \varphi(B)$  is a Borel set, so that  $\varphi^{-1}$  is a measurable function on  $\mathcal{B}$ . For  $I \in L^2(\Omega)$  and  $\varphi^{-1}$  as above, the concatenation  $I \circ \varphi^{-1} : \mathcal{B} \rightarrow \mathbb{R}$  is measurable if defined as follows

$$I \circ \varphi^{-1}(x) := \begin{cases} I \circ \varphi^{-1}(x), & x \in \mathcal{B}, \\ 0 & \text{otherwise.} \end{cases} \quad (5)$$

Then we get

$$\int_{\Omega} |I \circ \varphi^{-1}|^2 dx = \int_{\mathcal{B}} |I \circ \varphi^{-1}|^2 dx = \int_{\varphi^{-1}(\mathcal{B})} |I|^2 \det(D\varphi) dy,$$

which is finite since  $D\varphi$  has components in  $C^{0,\alpha}(\bar{\Omega})$ . This verifies (4). The same argument can be used to show that  $I \circ \varphi^{-1} \in L^p(\Omega)$ ,  $p \in [1, \infty)$  if  $I \in L^p(\Omega)$ . Further, the following lemma on the image of null sets under the mappings  $\varphi$  and  $\varphi^{-1}$  will be needed.

**Lemma 2.2.1.** *For  $\varphi \in \mathcal{A}$ , both  $\varphi$  and its pre-image mapping  $\varphi^{-1}$  map null sets to null sets.*

*Proof.* Since  $\varphi$  is Lipschitz continuous, it maps null sets to null sets, see [49, Theorem 3.33 and its proof].

Assume that there exists a Borel null set  $\mathcal{N}$  with  $\mu(\varphi^{-1}(\mathcal{N})) > 0$ . Then we obtain with characteristic function  $1_{\mathcal{N}}$  on  $\mathcal{N}$  the contradiction

$$0 = \int_{\mathcal{N}} 1_{\mathcal{N}} dx = \int_{\varphi^{-1}(\mathcal{N})} (1_{\mathcal{N}} \circ \varphi) |D\varphi| dy = \int_{\varphi^{-1}(\mathcal{N})} |D\varphi| dy > 0.$$

This finishes the proof. □

Finally, we prove a continuity result for the  $L^p$  norm with respect to mappings  $\varphi$  from  $\mathcal{A}$ .

**Lemma 2.2.2.** *Let  $I \in L^p(\Omega)$ ,  $p \in [1, \infty)$  and  $\{\varphi^{(j)}\}_{j \in \mathbb{N}}$  be a sequence of functions  $\varphi^{(j)} \in \mathcal{A}$  with  $\lim_{j \rightarrow \infty} \|\varphi^{(j)} - \hat{\varphi}\|_{(C^{1,\alpha}(\Omega))^n} = 0$  for some  $\hat{\varphi} \in \mathcal{A}$ . Then it holds*

$$\limsup_{j \rightarrow \infty} \|I \circ (\varphi^{(j)})^{-1} - I \circ \hat{\varphi}^{-1}\|_{L^p} = 0.$$

*Proof.* Since  $I \circ \hat{\varphi}^{-1} \in L^p(\Omega)$ , there exists a sequence  $\{I_k\}_{k \in \mathbb{N}}$  of uniformly continuous functions with  $\|I \circ \hat{\varphi}^{-1} - I_k\|_{L^p} \leq \frac{1}{k}$ . Then we conclude, using the fact that  $\varphi^{-1}$  maps null sets on null sets,

$$\begin{aligned} \|I \circ (\varphi^{(j)})^{-1} - I \circ \hat{\varphi}^{-1}\|_{L^p} &\leq \|I \circ (\varphi^{(j)})^{-1} - I_k \circ \hat{\varphi} \circ (\varphi^{(j)})^{-1}\|_{L^p} \\ &\quad + \|I_k \circ \hat{\varphi} \circ (\varphi^{(j)})^{-1} - I_k\|_{L^p} + \|I_k - I \circ \hat{\varphi}^{-1}\|_{L^p} \\ &\leq \left( \int_{\Omega} |I - I_k \circ \hat{\varphi}|^p \det(D(\varphi^{(j)})) \, dx \right)^{\frac{1}{p}} \\ &\quad + \left( \int_{\Omega} |I_k \circ \hat{\varphi} - I_k|^p \det(D(\varphi^{(j)})) \, dx \right)^{\frac{1}{p}} + \frac{1}{k}. \end{aligned}$$

Due to the convergence of  $\varphi^{(j)}$ , there exists a constant  $C$  such that  $\det(D(\varphi^{(j)})) \leq C$  for all  $j \in \mathbb{N}$ . Thus,

$$\begin{aligned} &\|I \circ (\varphi^{(j)})^{-1} - I \circ \hat{\varphi}^{-1}\|_{L^p} \\ &\leq \left( \int_{\Omega} |I - I_k \circ \hat{\varphi}|^p \det(D(\varphi^{(j)})) \, dx \right)^{\frac{1}{p}} + C \left( \int_{\Omega} |I_k \circ \hat{\varphi} - I_k|^p \, dx \right)^{\frac{1}{p}} + \frac{1}{k}. \end{aligned}$$

The last term goes to zero as  $k \rightarrow \infty$ . Fix  $k \in \mathbb{N}$ . Since  $\varphi^{(j)}$  converges uniformly to  $\hat{\varphi}$ , we can use the uniform continuity of  $I_k$  to conclude that  $I_k \circ \varphi^{(j)}$  converges uniformly to  $I_k \circ \hat{\varphi}$ . Then boundedness of  $\Omega$  implies that the second term converges to zero as  $j \rightarrow \infty$ . For the first term we obtain by the uniform continuity of  $I_k$  that for every  $\epsilon > 0$  there exists  $j \in \mathbb{N}$  large enough such that

$$\begin{aligned} \left( \int_{\Omega} |I - I_k \circ \hat{\varphi}|^p \det(D(\varphi^{(j)})) \, dx \right)^{\frac{1}{p}} &\leq \left( \int_{\Omega} |I - I_k \circ \hat{\varphi}|^p \det(D(\hat{\varphi})) \, dx \right)^{\frac{1}{p}} + \epsilon \\ &= \left( \int_{\Omega} |I \circ \hat{\varphi}^{-1} - I_k|^p \, dx \right)^{\frac{1}{p}} + \epsilon \\ &\leq \frac{1}{k} + \epsilon. \end{aligned}$$

This concludes the proof. □

### 3. Space Continuous Model

In this section, we establish our space continuous model, which takes the information I1) and I2) into account and prove that it has a minimizer.

#### 3.1. Model

Starting with the information I1), we are interested in reconstructing an original two-dimensional image from its measurements based on the variational approach (1). In this paper, we restrict our attention to the total variation semi-norm as regularizer  $\mathcal{P}$ . More precisely, recall that the space of functions of bounded variation  $BV(\Omega)$  consists

of those functions  $I \in L^1_{\text{loc}}(\Omega)$  having weak first order derivatives which are finite Radon measures. For  $I \in L^1(\Omega)$ , we know that  $I \in BV(\Omega)$  if and only if

$$TV(I) := \sup \left\{ \int_{\Omega} \text{Div}(\eta) \, dx : \eta \in (C_0^\infty(\Omega))^n, |\eta| \leq 1 \right\} < +\infty.$$

The space  $BV(\Omega)$  becomes a Banach space with the norm  $\|I\|_{BV} := \|I\|_{L^1} + TV(I)$ . For  $\Omega \subset \mathbb{R}^2$ , i.e.  $n = 2$ , the space  $BV(\Omega)$  can be continuously embedded into  $L^2(\Omega)$ , see [2, Theorem 3.47]. Therefore we can define

$$\mathcal{P}(I) := \begin{cases} TV(I) & \text{for } I \in BV(\Omega), \\ +\infty & \text{for } I \in L^2(\Omega) \setminus BV(\Omega). \end{cases} \quad (6)$$

We know that  $\mathcal{P}$  in (6) is a proper, convex and lower semi-continuous (lsc) functional on  $L^2(\Omega)$ , see [41, Proposition 10.8].

Let  $A : L^2(\Omega) \rightarrow \mathcal{Y}$  be a continuous linear operator into a Hilbert space  $\mathcal{Y}$  which does not vanish on constant functions and  $B \in \mathcal{Y}$ . For the Radon transform, we have for example  $\mathcal{Y} := L^2(\mathbb{S}^1, (-1, 1))$ . Then we set

$$\mathcal{E}(I; B) := \frac{1}{2} \|AI - B\|_{\mathcal{Y}}^2 + \alpha TV(I), \quad \alpha \geq 0. \quad (7)$$

Having a reference image  $R \in L^2(\Omega)$  available, we want to add this information to the model. To this end, let  $W : \mathbb{R}^{2,2} \rightarrow \mathbb{R}_{\geq 0}$  be a lsc mapping,  $\nu > 0$  and  $m > 2$ . Let  $K \geq 2$  be an integer. For a sequence  $\mathbf{I} := (I_0, \dots, I_{K-1})$  of images in  $L^2(\Omega)$  and a sequence of admissible mappings  $\boldsymbol{\varphi} := (\varphi_0, \dots, \varphi_{K-1})$  we consider the time discrete geodesic path model

$$\mathcal{F}(\mathbf{I}, \boldsymbol{\varphi}) := \sum_{k=0}^{K-1} \int_{\Omega} W(D\varphi_k) + \nu |D^m \varphi_k|^2 + |I_k \circ \varphi_k^{-1} - I_{k+1}|^2 \, dx, \quad (8)$$

where  $I_K := R \in L^2(\Omega)$  is a given reference image  $R \in L^2(\Omega)$ . Then our whole model reads

$$\mathcal{J}(\mathbf{I}, \boldsymbol{\varphi}) := \mathcal{F}(\mathbf{I}, \boldsymbol{\varphi}) + \beta \mathcal{E}(I_0; B) \quad \text{subject to } I_K = R, \quad (9)$$

where  $\beta > 0$ . We call this model TDM-INV model referring to 'time discrete morphing - inverse' problems.

**Remark 3.1.1.** *The linearized elastic potential will be our choice for  $W$  in (8). More precisely, rewriting the deformation as  $\varphi(x) = x + v(x)$  and introducing the notation of the (Cauchy) strain tensor of the displacement vector field  $v = (v_1, v_2)^T : \Omega \mapsto \mathbb{R}^2$  as*

$$Dv_{\text{sym}} := \begin{pmatrix} \partial_x v_1 & \frac{1}{2}(\partial_y v_1 + \partial_x v_2) \\ \frac{1}{2}(\partial_y v_1 + \partial_x v_2) & \partial_y v_2 \end{pmatrix},$$

we will apply

$$\mathcal{S}(v) := \int_{\Omega} \mu \, \text{trace} (Dv_{\text{sym}}^T Dv_{\text{sym}}) + \frac{\lambda}{2} \, \text{trace} (Dv_{\text{sym}})^2 \, dx, \quad \nu > 0. \quad (10)$$

Note that the linearized elastic potential is a usual regularizer in the context of registration, see [23, 30, 36].

### 3.2. Existence of a Minimizer

In this subsection, we show that  $\mathcal{J}(\mathbf{I}, \varphi)$  has a minimizer.

First, we fix an image sequence  $\mathbf{I} \in (L^2(\Omega))^K$  and show that  $J(\mathbf{I}, \cdot)$  has a minimizer  $\varphi \in \mathcal{A}^K$ . Then the consideration can be restricted to  $\mathcal{F}(\mathbf{I}, \cdot)$  and it suffices to prove that each of the summands

$$\mathcal{R}(\varphi_k; I_k, I_{k+1}) := \int_{\Omega} W(D\varphi_k) + \nu |D^m \varphi_k|^2 dx, + |I_k \circ \varphi_k^{-1} - I_{k+1}|^2 dx \quad (11)$$

$k = 0, \dots, K - 1$ , has a minimizer in  $\mathcal{A}$ .

**Theorem 3.2.1.** *Let  $W: \mathbb{R}^{n,n} \rightarrow \mathbb{R}_{\geq 0}$  be a lsc mapping with the property*

$$W(M) = \infty \quad \text{if} \quad \det M \leq 0. \quad (12)$$

*Further, let  $R \in L^2(\Omega)$  be given. Then there exists a minimizer  $\hat{\varphi} \in \mathcal{A}$  of*

$$\mathcal{R}(\varphi; T, R) := \int_{\Omega} W(D\varphi) + \nu |D^m \varphi|^2 + |T \circ \varphi^{-1}(x) - R(x)|^2 dx$$

*over all  $\varphi \in \mathcal{A}$ .*

The proof applies similar ideas as in [7, 32]. However, since the setting in those papers was different, we prefer to carefully follow the lines and make the necessary modifications.

*Proof.* Let  $\{\varphi^{(j)}\}_j$ ,  $\varphi^{(j)} \in \mathcal{A}$ , be a minimizing sequence of  $\mathcal{R}$ . Then we have that  $\mathcal{R}(\varphi^{(j)}; T, R) \leq C$  for all  $j \in \mathbb{N}$ . This implies that  $\{\varphi^{(j)}\}_j$  has uniformly bounded  $(W^{m,2}(\Omega))^n$  semi-norm, and by (3) the sequence is also uniformly bounded in  $(L^2(\Omega))^n$ . Now we apply the Gagliardo-Nirenberg inequality, Theorem A.0.1 in the form given in Remark A.0.2, which states that for all  $0 \leq i < m$  it holds

$$\|D^i \varphi^{(j)}\|_{L^2(\Omega)} \leq C_1 \|D^m \varphi^{(j)}\|_{L^2(\Omega)} + C_2 \|\varphi^{(j)}\|_{L^2(\Omega)}, \quad \nu = 1, \dots, n.$$

All terms on the right-hand side are uniformly bounded. Hence, the  $(W^{m,2}(\Omega))^n$  norm of  $\{\varphi^{(j)}\}_j$  is uniformly bounded. Since  $W^{m,2}(\Omega)$  is reflexive, there exists a subsequence which converges weakly to some function  $\hat{\varphi}$  in  $(W^{m,2})^n$ . By the compact embedding  $W^{m,2}(\Omega) \hookrightarrow C^{1,\alpha}(\bar{\Omega})$ ,  $\alpha \in (0, m - 1 - \frac{n}{2})$ , this subsequence, which we denote by  $\{\varphi^{(j)}\}_j$  again, converges strongly to  $\hat{\varphi}$  in  $(C^{1,\alpha}(\bar{\Omega}))^n$  and  $D\varphi^{(j)}$  converges uniformly to  $D\hat{\varphi}$ .

Next we show that  $\hat{\varphi}$  is in the set  $\mathcal{A}$ . Since  $W$  is lsc, we conclude

$$\liminf_{j \rightarrow \infty} W(D\varphi^{(j)})(x) \geq W(D\hat{\varphi})(x)$$

for all  $x \in \Omega$  and since  $W$  is nonnegative we obtain by Fatou's lemma

$$\int_{\Omega} W(D\hat{\varphi}(x)) dx \leq \liminf_{j \rightarrow \infty} \int_{\Omega} W(D\varphi^{(j)}(x)) dx \leq C.$$

By (12) this implies  $\det(D\hat{\varphi}(x)) > 0$  a.e.. Further the boundary condition is fulfilled so that  $\hat{\varphi} \in \mathcal{A}$ .

It remains to show  $\lim_{j \rightarrow \infty} \mathcal{R}(\varphi^{(j)}; T, R) = \mathcal{R}(\hat{\varphi}; T, R)$ . By Lemma 2.2.2, we know  $\|T \circ (\varphi^{(j)})^{-1} - T \circ \hat{\varphi}^{-1}\|_{L^2} \rightarrow 0$  as  $j \rightarrow \infty$ , so that by the continuity of the norm

$$\|T \circ \hat{\varphi}^{-1} - R\|_{L^2} = \lim_{j \rightarrow \infty} \|T \circ (\varphi^{(j)})^{-1} - R\|_{L^2}.$$

This together with the previous steps of the proof implies that the three summands in  $\mathcal{R}$  are (weakly) lsc. We get

$$\begin{aligned} \mathcal{R}(\hat{\varphi}; T, R) &\leq \liminf_{j \rightarrow \infty} \int_{\Omega} W(D\varphi^{(j)}) + \nu |D^m \varphi^{(j)}|^2 + |T \circ (\varphi^{(j)})^{-1} - R|^2 dx \\ &= \inf_{\varphi \in \mathcal{A}} \mathcal{R}(\varphi) \end{aligned}$$

which proves the claim.  $\square$

Next, we fix a sequence of mappings  $\varphi \in \mathcal{A}^K$  and ask for a minimizer of  $\mathcal{J}(\cdot, \varphi)$ .

**Theorem 3.2.2.** *Let  $A : L^2(\Omega) \rightarrow \mathcal{Y}$  be a continuous linear operator into a Hilbert space  $\mathcal{Y}$  which does not vanish on constant functions and  $B \in \mathcal{Y}$ . For fixed  $\varphi \in \mathcal{A}^K$ , there exists a unique image sequence  $\mathbf{I} \in (L^2(\Omega))^K$  which minimizes  $\mathcal{J}(\cdot, \varphi)$ .*

*Proof.* Neglecting the constant terms it remains to consider

$$J(\mathbf{I}) := \sum_{k=1}^{K-1} \int_{\Omega} |I_k \circ \varphi_k^{-1}(x) - I_{k+1}(x)|^2 dx + \beta \mathcal{E}(I_0; B) \quad \text{subject to} \quad I_K = R. \quad (13)$$

Setting

$$\begin{aligned} \psi_0(y) &:= y, \\ \psi_k(y) &:= \varphi_{k-1} \circ \psi_{k-1}(y) = \varphi_{k-1} \circ \dots \circ \varphi_0(y), \quad k = 1, \dots, K, \end{aligned} \quad (14)$$

and substituting  $x := \psi_k(y)$  in the  $k$ -th summand of (13), we obtain

$$J(\mathbf{I}) = \sum_{k=1}^K \int_{\Omega} |I_k(\psi_k(x)) - I_{k-1}(\psi_{k-1}(x))|^2 \det(D\psi_k(x)) dx + \beta \mathcal{E}(I_0; B).$$

Using  $\mathbf{F} := (F_0, \dots, F_{K-1})$ , where  $F_0 := I_0$ ,  $F_k := I_k \circ \psi_k$ , and  $w_0(x) := 1$ ,  $w_k(x) := \det(D\psi_k(x))$ ,  $k = 1, \dots, K$ . We are concerned with the minimization of

$$\begin{aligned} \tilde{J}(\mathbf{F}) &:= \sum_{k=1}^K \int_{\Omega} |F_k(x) - F_{k-1}(x)|^2 w_k(x) dx + \beta \mathcal{E}(F_0; B) \\ &\text{subject to} \quad F_K = R \circ \psi_K. \end{aligned} \quad (15)$$

Note that by  $0 < w_k(x) \leq C$  a.e.,  $k = 1, \dots, K$  and  $w_k = w_{k-1} \det(D\varphi_{k-1})$ , we have for the weighted  $L^2$  spaces

$$L^2(\Omega) = L^2_{w_0}(\Omega) \subseteq L^2_{w_1}(\Omega) \subseteq \dots \subseteq L^2_{w_K}(\Omega), \quad (16)$$

in particular  $F_K \in L^2_{w_K}(\Omega)$  if  $R \in L^2(\Omega)$ . A minimizer must fulfill  $F_0 \in BV(\Omega) \subset L^2(\Omega)$ , and by successively considering the integrals in (15) further  $F_k \in L^2_{w_k}(\Omega)$ ,  $k = 1, \dots, K$ . Since the function  $g : \mathbb{R}^K \rightarrow \mathbb{R}$ ,

$$g(f_0, \dots, f_{K-1}) := \sum_{k=1}^K (f_k - f_{k-1})^2 w_k$$

with  $w_k > 0$ ,  $k = 1, \dots, K$  and  $f_K$  fixed, is strictly convex, we have that the sum of the integrals in  $\tilde{J}$  is strictly convex. Clearly, this sum which can be rewritten as  $\sum_{k=1}^{K-1} \|F_k - F_{k-1}\|_{L^2_{w_k}} + \|R \circ \psi_K - F_{K-1}\|_{L^2_{w_K}}$  is continuous. Since  $\mathcal{E}(F_0; B)$  is proper, convex and lsc, we obtain that the same holds true for  $\tilde{J}$  over  $L^2_{w_0}(\Omega) \times \dots \times L^2_{w_{K-1}}(\Omega)$ . Thus,  $\tilde{J}$  is also weakly lsc, see [41, Lemma 10.4].

Next we show that  $\tilde{J}$  is coercive. Assume conversely that  $\sum_{k=0}^{K-1} \|F_k^{(j)}\|_{L^2_{w_k}} \rightarrow \infty$  but  $\tilde{J}(\mathbf{F}^{(j)})$  is bounded. By assumption on  $A$  we know that  $\mathcal{E}(F_0; B)$  is coercive, see [10, Theorem 6.115]. Thus,  $\|F_0^{(j)}\|_{L^2}$  is bounded and by (16) also  $\|F_0^{(j)}\|_{L^2_{w_1}}$  is bounded which implies by assumption on  $\tilde{J}$  that  $\|F_1^{(j)}\|_{L^2_{w_1}}$  is bounded. Considering successively the integrals in (15) we obtain  $\|F_k^{(j)}\|_{L^2_{w_k}}$ ,  $k = 1, \dots, K-1$  is bounded which contradicts our assumption.

Thus,  $\tilde{J}$  is coercive and together with its weak lsc property and the strict convexity, we conclude that the functional has a unique minimizer  $\mathbf{F}$ . By definition of  $\mathbf{F}$  we get the unique minimizer  $\mathbf{I}$  with  $I_k = F_k \circ \psi_k^{-1} \in L^2(\Omega)$  of  $J$ .  $\square$

For our computations, the following corollary on the minimizer of first part of the functional  $\tilde{J}$  in (15) will be useful.

**Corollary 3.2.3.** *Let  $K \geq 2$  be an integer. Let  $w_k \in C^{0,\alpha}(\bar{\Omega})$ ,  $k = 1, \dots, K$  fulfill  $w_k > 0$  a.e. on  $\Omega$  and  $\frac{w_{k+1}}{w_k} \leq C$ ,  $k = 1, \dots, K-1$ . For given  $F_0 \in L^2(\Omega)$  and  $F_K \in L^2_{w_K}(\Omega)$ , the solution of*

$$\arg \min_{F_k \in L^2_{w_k}} \sum_{k=2}^{K-1} \int_{\Omega} |F_k(x) - F_{k-1}(x)|^2 w_k(x) dx$$

is given by

$$F_k(x) = t_k F_0 + (1 - t_k) F_K, \quad t_k := \frac{\sum_{i=1}^k w_i^{-1}}{\sum_{i=1}^K w_i^{-1}}. \quad (17)$$

*Proof.* Setting the first derivative of the functional to zero we obtain a.e. on  $\Omega$ ,

$$w_k(F_k - F_{k-1}) + w_{k+1}(F_k - F_{k+1}) = 0, \quad k = 1, \dots, K-1$$

a.e. on  $\Omega$ . This can be rewritten as linear system of equations

$$\text{tridiag}(-w_k, w_k + w_{k+1}, -w_{k+1})_{k=1}^{K-1} (F_1, \dots, F_{K-1})^T = (w_1 F_0, 0, \dots, 0, w_K F_K)^T.$$

Since the tridiagonal matrix is irreducible diagonal dominant, the system has a unique solution. Straightforward computation shows that the solution is given by (17).  $\square$

Finally, we can prove the main result of this section.

**Theorem 3.2.4.** *Let  $R \in L^2(\Omega)$  and  $K \geq 2$ . Then there exists a sequence  $(\hat{\mathbf{I}}, \hat{\varphi}) \in L^2(\Omega)^K \times \mathcal{A}^K$  minimizing  $\mathcal{J}$ .*

*Proof.* 1. Let  $\{(\mathbf{I}^{(j)}, \phi^{(j)})\}_{j \in \mathbb{N}}$  be a minimizing sequence of  $\mathcal{J}$ . Then

$\mathcal{J}(\mathbf{I}^{(j)}, \phi^{(j)}) \leq C$  for all  $j \in \mathbb{N}$ . By Theorem 3.2.1, we find for each  $\mathbf{I}^{(j)}$  a sequence of diffeomorphisms  $\varphi^{(j)}$  such that

$$\mathcal{J}(\mathbf{I}^{(j)}, \varphi^{(j)}) \leq \mathcal{J}(\mathbf{I}^{(j)}, \varphi)$$

for all  $\varphi \in \mathcal{A}^K$ . Then we know  $\|D^m \varphi_k^{(j)}\|_{L^2(\Omega)}^2 < \frac{1}{\nu} C$  for all  $j \in \mathbb{N}$  and  $k = 0, \dots, K-1$ .

As in the first part of the proof of Theorem 3.2.1 we conclude that  $\{\varphi_k^{(j)}\}_j$  is bounded in  $(W^{m,2}(\Omega))^n$ , so that there exists a subsequence converging weakly in  $(W^{m,2}(\Omega))^n$  and strongly in  $(C^{1,\alpha}(\bar{\Omega}))^n$ ,  $0 < \alpha < m-1-\frac{n}{2}$  to  $\hat{\varphi}_k$ . Set  $\hat{\varphi} := (\hat{\varphi}_k)_{k=0}^{K-1}$ . Let us denote this subsequence again by  $\{\varphi_k^{(j)}\}_j$  and  $\varphi^{(j)} := (\varphi_k^{(j)})_{k=1}^K$ .

2. Since  $\mathcal{J}(\mathbf{I}^{(j)}, \varphi^{(j)}) \leq C$  for all  $j \in \mathbb{N}$ , we conclude

$$\begin{aligned} \|I_{k+1}^{(j)}\|_{L^2} &\leq \|I_k^{(j)} \circ (\varphi_k^{(j)})^{-1} - I_{k+1}^{(j)}\|_{L^2} + \|I_k^{(j)} \circ (\varphi_k^{(j)})^{-1}\|_{L^2} \\ &\leq C + \|I_k^{(j)} \circ (\varphi_k^{(j)})^{-1}\|_{L^2}. \end{aligned}$$

Since  $\varphi_k^{(j)}$  is convergent in  $(C^{1,\alpha}(\bar{\Omega}))^n$  we obtain  $|\det(D\varphi_k^{(j)})| \leq \tilde{C}$  on  $\Omega$  for  $k = 1, \dots, K-1$ , Then we get

$$\begin{aligned} \|I_1^{(j)}\|_{L^2} &\leq C + \|I_0 \circ (\varphi_0^{(j)})^{-1}\|_{L^2(\Omega)} \\ \|I_2^{(j)}\|_{L^2} &\leq C + \|I_1 \circ (\varphi_1^{(j)})^{-1}\|_{L^2} \\ &= C + \left( \int_{\Omega} |I_1^{(j)}(x)|^2 |\det(D\varphi_1^{(j)}(x))| dx \right)^{\frac{1}{2}} \\ &\leq C + \tilde{C}^{\frac{1}{2}} \|I_1^{(j)}\|_{L^2} \end{aligned}$$

Successive continuation shows that the sequence  $\{\mathbf{I}^{(j)}\}_{j \in \mathbb{N}}$  is bounded in  $(L^2(\Omega))^K$ . Hence, there exists a weakly convergent subsequence, also denoted by  $\{\mathbf{I}^{(j)}\}_{j \in \mathbb{N}}$ , which converges to  $\hat{\mathbf{I}} \in (L^2(\Omega))^K$ .

3. Next, we show the weak convergence of  $I_k^{(j)} \circ (\varphi_k^{(j)})^{-1}$  to  $\hat{I}_k \circ (\hat{\varphi}_k)^{-1}$ . For all  $g \in L^2(\Omega)$ , it holds

$$\int_{\Omega} \left( I_k^{(j)} \circ (\varphi_k^{(j)})^{-1}(x) - \hat{I}_k \circ (\hat{\varphi}_k)^{-1}(x) \right) g(x) dx = \mathcal{I}_1^{(j)} + \mathcal{I}_2^{(j)}$$

with

$$\begin{aligned}\mathcal{I}_1^{(j)} &:= \int_{\Omega} \left( I_k^{(j)} \circ (\varphi_k^{(j)})^{-1}(x) - I_k^{(j)} \circ (\hat{\varphi}_k)^{-1}(x) \right) g(x) dx, \\ \mathcal{I}_2^{(j)} &:= \int_{\Omega} \left( I_k^{(j)} \circ (\hat{\varphi}_k)^{-1}(x) - \hat{I}_k \circ (\hat{\varphi}_k)^{-1}(x) \right) g(x) dx.\end{aligned}$$

Using the transformation formula, we obtain

$$\mathcal{I}_2^{(j)} = \int_{\Omega} \left( I_k^{(j)}(x) - \hat{I}_k(x) \right) \det(D\hat{\varphi}_k(x)) g(\hat{\varphi}_k(x)) dx.$$

Since  $\det(D\hat{\varphi}_k)(g \circ \hat{\varphi}_k) \in L^2$ , we conclude by the weak convergence of the  $I_k^{(j)}$  to  $\hat{I}_k$  that  $\mathcal{I}_2^{(j)}$  converges to zero as  $j \rightarrow \infty$ . Using the transformation formula again, we get

$$\begin{aligned}\mathcal{I}_1^{(j)} &= \int_{\Omega} I_k^{(j)}(x) \left( g \circ \varphi_k^{(j)}(x) \det(D\varphi_k^{(j)}(x)) - g \circ \hat{\varphi}_k(x) \det(D\hat{\varphi}_k(x)) \right) dx \\ &\leq \left\| I_k^{(j)} \right\|_{L^2} \left\| g \circ \varphi_k^{(j)} \det(D\varphi_k^{(j)}) - g \circ \hat{\varphi}_k \det(D\hat{\varphi}_k) \right\|_{L^2}.\end{aligned}$$

Since  $\{I_k^{(j)}\}_j$  is bounded, it suffices to show the convergence of the second factor. Using that  $C_0^\infty(\Omega)$  is dense in  $L^2(\Omega)$ , we may assume that  $g \in C_0^\infty(\Omega)$ . Then, it follows with  $g_k^{(j)} := g \circ \varphi_k^{(j)}$  and  $\hat{g}_k := g \circ \hat{\varphi}_k$  that

$$\begin{aligned}& \left\| g_k^{(j)} \det(D\varphi_k^{(j)}) - \hat{g}_k \det(D\hat{\varphi}_k) \right\|_{L^2} \\ & \leq \left\| g_k^{(j)} \det(D\varphi_k^{(j)}) - g_k^{(j)} \det(D\hat{\varphi}_k) \right\|_{L^2} + \left\| g_k^{(j)} \det(D\hat{\varphi}_k) - \hat{g}_k \det(D\hat{\varphi}_k) \right\|_{L^2} \\ & \leq C \left\| \det(D\varphi_k^{(j)}) - \det(D\hat{\varphi}_k) \right\|_{L^2} + C \|g_k^{(j)} - \hat{g}_k\|_{L^2}.\end{aligned}$$

The first term converges to zero since  $D\varphi_k^{(j)}$  is strongly convergent. Strong convergence of  $\varphi_k^{(j)}$  also implies together with the uniform continuity of  $g$ , that  $g_k^{(j)}$  converges uniformly to  $\hat{g}_k$ . Now boundedness of  $\Omega$  implies that the second term converges to zero.

4. Finally, we consider

$$\begin{aligned}\liminf_{j \rightarrow \infty} \mathcal{J}(\mathbf{I}^{(j)}, \varphi^{(j)}) &\geq \sum_{k=0}^{K-1} \liminf_{j \rightarrow \infty} \int_{\Omega} W(D\varphi_k^{(j)}) dx + \nu \liminf_{j \rightarrow \infty} \int_{\Omega} |D^m \varphi_k^{(j)}|^2 dx \\ &\quad + \liminf_{j \rightarrow \infty} \|I_k^{(j)} \circ (\varphi_k^{(j)})^{-1} - I_{k+1}^{(j)}\|_{L^2}^2\end{aligned}$$

We use that the components of  $\varphi_k^{(j)}$  weakly converge in  $W^{m,2}(\Omega)$ , those of  $D\varphi_k^{(j)}$  strongly converge in  $C^{0,\alpha}(\Omega)$ , and  $I_k^{(j)}$ ,  $I_k^{(j)} \circ (\varphi_k^{(j)})^{-1}$  weakly converge in  $L^2(\Omega)$  together with the fact that the first summand is lsc and the second one weakly lsc and  $\|f - g\|_{L^2}^2$  is weakly lsc (convex and lsc) in both arguments to get

$$\inf \mathcal{J}(\mathbf{I}, \phi) = \liminf_{j \rightarrow \infty} \mathcal{J}(\mathbf{I}^{(j)}, \phi^{(j)}) \geq \liminf_{j \rightarrow \infty} \mathcal{J}(\mathbf{I}^{(j)}, \varphi^{(j)}) \geq \mathcal{J}(\hat{\mathbf{I}}, \hat{\varphi}).$$

This finishes the proof.  $\square$

## 4. Minimization Algorithm

To minimize  $\mathcal{J}(\mathbf{I}, \varphi)$  we apply a minimization scheme which alternates over the admissible sequence of deformations

$\varphi := (\varphi_0, \dots, \varphi_{K-1})$  and the sequence of images  $\mathbf{I} := (I_0, \dots, I_{K-1})$ . Starting with  $\mathbf{I}^{(0)}$  we iterate for  $j = 0, \dots$ :

1. For  $k = 0, 1, \dots, K - 1$ , we compute

$$\varphi_k^{(j)} := \arg \min_{\varphi_k} \left\{ \int_{\Omega} W(D\varphi_k) + \nu |D^m \varphi_k|^2 + |I_k^{(j)} \circ \varphi_k^{-1} - I_{k+1}^{(j)}|^2 dx \right\}. \quad (18)$$

2. For given  $A \in L(L^2(\Omega), \mathcal{Y})$ ,  $B \in \mathcal{Y}$  and  $R \in L^2(\Omega)$ , we solve

$$\mathbf{I} := \arg \min_{\mathbf{I}} \left\{ \sum_{k=0}^{K-2} \|I_k \circ (\varphi_k^{(j)})^{-1} - I_{k+1}\|_{L^2}^2 + \|I_{K-1} \circ (\varphi_{K-1}^{(j)})^{-1} - R\|_{L^2}^2 + \frac{\beta}{2} \|AI_0 - B\|_{\mathcal{Y}}^2 + \alpha \beta TV(I_0) \right\}. \quad (19)$$

Then, for the alternating process, the sequence of functional values  $\{\mathcal{J}(\varphi^{(j)}, \mathbf{I}^{(j)})\}_j$  decreases. By the analysis of the previous section, the sequence  $\{(\varphi^{(j)}, \mathbf{I}^{(j)})\}_j$  is bounded so that at least the weak convergence of a subsequence can be guaranteed. So far, we have not proved the strong convergence of the whole sequence to a (local) minimizer.

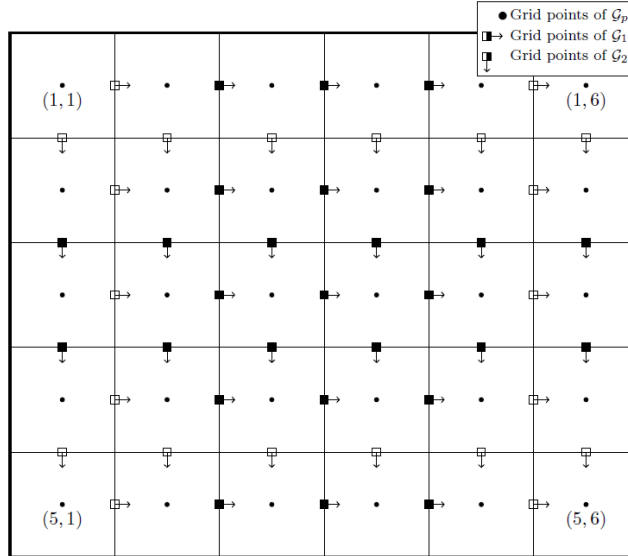


Figure 2: Illustration of the staggered grid, where empty boxes mean zero movement.

### 4.1. Spatial Discretization

In practice, we have to work in a spatially discrete setting. Dealing with rectangular digital images, we propose a finite difference approach, where we work on staggered grids,

see Fig. 2. For an application of mimetic grid techniques in optical flow computation see also [51]. In the following, we briefly sketch the space discrete approach.

The domain of the images  $I$  is the (primal) grid  $\mathcal{G} := \{1, \dots, n_1\} \times \{1, \dots, n_2\}$ . All integrals are approximated on the integration domain  $\bar{\Omega} := [\frac{1}{2}, n_1 + \frac{1}{2}] \times [\frac{1}{2}, n_2 + \frac{1}{2}]$  by the midpoint quadrature rule, i.e., with pixel values defined on  $\mathcal{G}$ .

As function  $W(D\varphi)$  we use the linearized elastic potential  $\mathcal{S}(v)$  in Remark 3.1.1 with the replacement  $v = (v_1, v_2)^T = \varphi - \text{id}$ . Using the  $\frac{1}{2}$ -shifted grids

$$\mathcal{G}_1 := \{\frac{3}{2}, \dots, n_1 - \frac{1}{2}\} \times \{1, \dots, n_2\}, \quad \mathcal{G}_2 := \{1, \dots, n_1\} \times \{\frac{1}{2}, \dots, n_2 - \frac{3}{2}\},$$

we consider  $v = (v_1, v_2)^T$  with  $v_1: \mathcal{G}_1 \rightarrow \mathbb{R}$  and  $v_2: \mathcal{G}_2 \rightarrow \mathbb{R}$ . Then, the spatially discrete version of  $\mathcal{S}$  reads

$$\begin{aligned} \mathcal{S}(v) = & \mu \left( \|D_{1,x_1} v_1\|_F^2 + \|v_2 D_{2,x_2}^T\|_F^2 + \frac{1}{2} \|v_1 D_{1,x_2}^T + D_{2,x_1} v_2\|_F^2 \right) \\ & + \frac{\lambda}{2} \|D_{1,x_1} v_1 + v_2 D_{2,x_2}^T\|_F^2, \end{aligned}$$

where  $\|\cdot\|_F$  is the Frobenius norm of matrices and  $D_{i,x_j}$  denotes the forward differences operator (matrix) for  $v_i$  in  $x_j$ -direction. The higher order term  $\int_{\Omega} |D^m \varphi|^2 dx$  with  $m = 3$  is discretized by

$$\mathcal{D}_3(v) := \sum_{i=0}^3 \|D_{1,x_1}^i v_1 D_{1,x_2}^{3-i}\|_F^2 + \|D_{2,x_1}^i v_2 D_{2,x_2}^{3-i}\|_F^2 + \eta (\|v_1\|_F^2 + \|v_2\|_F^2),$$

where we use central differences operators for the partial derivatives of order two and three. Note that we have added the squared Frobenius norm of the  $v_i$ ,  $i = 1, 2$  to better control the displacement value. To cope with the remaining term in (18), we approximate  $\varphi^{-1} \approx \text{id} - v$  such that the data term becomes

$$\int_{\Omega} |I_k^{(j)}(x - v(x)) - I_{k+1}^{(j)}(x)|^2 dx. \quad (20)$$

We evaluate this integral using again the midpoint quadrature rule. Since  $v_i$  is only defined on  $\mathcal{G}_i$ ,  $i = 1, 2$  and not on  $\mathcal{G}$ , we use instead of  $v$  its bilinear interpolation at the grid points, i.e., the averaged version  $Pv = (P_1 v_1, P_2 v_2)^T: \mathcal{G} \rightarrow \mathbb{R}^2$ . In general  $x - Pv(x) \notin \mathcal{G}$ , so that the image  $I_k(x - Pv(x))$  has to be interpolated from its values on  $\mathcal{G}$ . Here we use spline interpolation with Akima splines [16]. For simplicity, we keep the notation  $I_k$ .

Summarizing, the functionals in (18) become

$$\mathcal{R}(v_k; I_k^{(j)}, I_{k+1}^{(j)}) := \mathcal{S}(v_k) + \nu \mathcal{D}_3(v_k) + \sum_{x \in \mathcal{G}} |I_k^{(j)}(x - Pv_k(x)) - I_{k+1}^{(j)}(x)|^2, \quad (21)$$

for  $k = 0, \dots, K - 1$ . We apply a Quasi-Newton method to find minimizers of all these functionals. The method is described in detail in [32], see also [36].

For the computation of the image sequence in the second step of the alternating minimization process we use the substitution in the proof of Theorem 3.2.2. Setting  $\psi_k := \varphi_{k-1} \circ \dots \circ \varphi_0$ ,  $w_k(x) := \det(D\psi_k(x))$  and  $F_0 := I_0$ ,  $F_k := I_k \circ \psi_k$ ,  $k = 1, \dots, K$ , we can transform (19) to the problem

$$\arg \min_{\mathbf{F}} \left\{ \sum_{k=0}^{K-1} \|(F_k - F_{k+1})\sqrt{w_{k+1}}\|_{L^2}^2 + \frac{\beta}{2} \|AF_0 - B\|_{\mathcal{Y}}^2 + \alpha\beta TV(F_0) \right\} \quad (22)$$

and discretize the functional on  $\mathcal{G}$ , using again the midpoint rule for the integral. Note that  $F_K$  is known. For the TV-term we use the forward differences  $D_{x_i}$  in  $x_i$ ,  $i = 1, 2$  direction

$$TV(I) := \left\| \sqrt{(D_{x_1}I)^2 + (ID_{x_2}^T)^2} \right\|_1,$$

where the square and the square root are meant componentwise, and  $\|\cdot\|_1$  is the sum of the entries of the matrix. If  $F_0$  is fixed, then by Corollary 3.2.3 the minimizer of the first summand is given analytically. Therefore we propose an alternating algorithm which fixes alternately  $F_0$  and  $\bar{\mathbf{F}} := (F_1, \dots, F_{K-1})$ . This alternating method is also known as block-coordinate descent and the following convergence result was proved in [4, Theorem 14.9, Theorem 14.15], see also [5].

**Theorem 4.1.1.** *Let  $E_1, E_2$  be Euclidean spaces and  $G : E_1 \times E_2 \rightarrow \mathbb{R} \cup \{+\infty\}$ ,  $G_i : E_i \rightarrow \mathbb{R} \cup \{+\infty\}$ ,  $i = 1, 2$  be proper, convex lsc functions. Assume further that  $G$  is continuously differentiable and that the level sets of  $G + G_1 + G_2$  are bounded. Then the minimization problem*

$$\arg \min_{x_1, x_2} \{G(x_1, x_2) + G_1(x_1) + G_2(x_2)\}$$

can be solved by alternating minimization in  $x_1$  and  $x_2$ , i.e., every accumulation point of the generated iteration sequence is a minimizer. The convergence rate for the functional values is  $\mathcal{O}(\frac{1}{k})$ .

For our specific discretized problem (22) with

$$\begin{aligned} G(F_0, \bar{\mathbf{F}}) &:= \sum_{x \in \mathcal{G}} |F_0(x) - F_1(x)|^2 w_1(x), \\ G_1(\bar{\mathbf{F}}) &:= \sum_{k=0}^{K-1} \sum_{x \in \mathcal{G}} |F_k(x) - F_{k+1}(x)|^2 w_{k+1}(x), \\ G_2(F_0) &:= \frac{\beta}{2} \|AF_0 - B\|_{\mathcal{Y}}^2 + \alpha\beta TV(F_0), \end{aligned}$$

the conditions of the theorem are obviously fulfilled. If  $F_0$  is fixed, Corollary 3.2.3 implies that the minimizer of  $G(F_0, \bar{\mathbf{F}}) + G_1(\bar{\mathbf{F}})$  is given analytically. In the second step of the algorithm, we have to minimize, for fixed  $\bar{\mathbf{F}}$ , i.e., fixed  $F_1$ , the functional

$$G(F_0, \bar{\mathbf{F}}) + G_2(F_0) := \sum_{x \in \mathcal{G}} |F_0(x) - F_1(x)|^2 w_1(x) + \frac{\beta}{2} \|AF_0 - B\|_{\mathcal{Y}}^2 + \alpha\beta TV(F_0). \quad (23)$$

This can be done efficiently by primal-dual algorithms from convex analysis as for example by the Chambolle-Pock algorithm [12, 37] or the parallel Douglas-Rachford algorithm [9]. Indeed there is a vast literature how to solve problems of this kind. For an overview we refer, e.g. to [11, 13]. Finally, we use scattered interpolation to obtain the images in  $\mathbf{I}$  at grid points from  $\mathbf{F}$ .

**Remark 4.1.2.** *Instead of using the the transformed version  $\mathbf{F}$ , we can also compute a solution of*

$$\arg \min_{\mathbf{I}} \left\{ \sum_{k=0}^{K-1} \sum_{x \in \mathcal{G}} |(I_k(x - v(x)) - I_{k+1}(x))|^2 + \frac{\beta}{2} \|AI_0 - B\|_{\mathcal{Y}}^2 + \alpha\beta TV(I_0) \right\}$$

for the  $\mathbf{I}$  directly. Bilinear interpolation of the  $I_k(x)$ ,  $x \in \mathbb{R}^2$  results in a linear combination of bilinear basis functions. Thus, applying the quadrature rule in (20), the minimization can be done via the coefficients of the linear combinations which also leads to the solution of triangular linear systems of equations with respect to the coefficients.

## 4.2. Multilevel approach

As usual in optical flow and image registration, we apply a coarse-to-fine strategy with  $\text{lev} \in \mathbb{N}$  levels. First, we iteratively smooth our given images by convolution with a truncated Gaussian and downsampling using bilinear interpolation. Here special care is necessary for the operator  $A$ , as well as for the downsampling procedure of the data  $B$ , which is dependent on the operator choice. Both procedures are described in the respective numerical examples.

To obtain a deformation on the coarsest level we perform a single registration with the solution of the  $L^2$ -TV problem, i.e.,

$$I_{0,\text{lev}} = \arg \min_{I: \mathcal{G}_{\text{lev}} \rightarrow \mathbb{R}} \left\{ \frac{1}{2} \|A_{\text{lev}}I - B_{\text{lev}}\|^2 + \alpha TV(I) \right\}, \quad \alpha > 0, \quad (24)$$

where  $\text{lev} \in \mathbb{N}$  is number of levels. For better results we decrease the regularization parameters for  $v$  as recommended by Modersitzki [31].

Then, we apply bilinear interpolation to construct a deformation on the next finer level. The sequence of  $\tilde{K} - 1$ ,  $\tilde{K} < K$ , intermediate finer level images is initialized from the end

$$I_k(x) = R\left(x + \frac{k}{\tilde{K}} Pv(x)\right), \quad (25)$$

where  $R$  is the end image at the current level. Using this we obtain an initial image sequence on this level. Then we start the alternating minimization to obtain better deformations and intermediate images. We go to the next finer level by bilinear interpolation of the deformation and image sequence. Then we construct more intermediate images by deforming the images from behind similar to (25), i.e., to get new images between  $I_k$  and  $I_{k+1}$  we use the later image  $I_{k+1}$ . We repeat this procedure until we reach the maximal number  $K$  of images and the finest level. The complete multilevel strategy is sketched in Algorithm 1.

---

**Algorithm 1** TDM-INV Algorithm (informal)

---

```
1:  $R_0 := R, B_0 := B, \mathcal{G}_0 := \mathcal{G}$ 
2: create image stack  $(R_l)_{l=0}^{\text{lev}}, (B_l)_{l=0}^{\text{lev}}$  on  $(\mathcal{G}_l)_{l=0}^{\text{lev}}$  by downsampling
3: solve (24) for  $B_{\text{lev}}$ 
4: solve (21) for  $R_{\text{lev}}, I_{0,\text{lev}}$  to get  $\tilde{v}$ 
5:  $l \rightarrow \text{lev} - 1$ 
6: use bilinear interpolation to get  $v$  on  $\mathcal{G}_l$  from  $\tilde{v}$ 
7: obtain  $\tilde{K}_l$  images  $\mathbf{I}_l^{(0)}$  from  $R_l, v$  by (25)
8: while  $l \geq 0$  do
9:   repeat(Alternating outer iteration)
10:    find deformations  $\tilde{\mathbf{v}}_l^{(i+1)}$  minimizing (21) for every pair from  $\mathbf{I}_l^{(i)}$ 
11:    initialize  $\mathbf{F}^{(0)} = \mathbf{I}_l^{(i)}$ 
12:    repeat(Alternating inner iteration)
13:      For fixed  $F_0^{(j)}$  compute  $F_1^{(j+1)}, \dots, F_{K-1}^{(j+1)}$  according to Corollary 3.2.3
14:      For fixed  $F_1^{(j+1)}$  compute  $F_0^{(j+1)}$  as solution of (23) using a PD-method
15:       $j \rightarrow j + 1$ 
16:    until convergence criterion is reached
17:    compute  $\mathbf{I}_l^{(i)}$  from  $F^{(j)}$  using scattered interpolation
18:     $i \rightarrow i + 1$ 
19:  until convergence criterion is reached
20:   $l \rightarrow l - 1$ 
21:  if  $l > 0$  then
22:    use bilinear interpolation to get  $\mathbf{I}_l$  and  $\mathbf{v}_l$  on  $\mathcal{G}_l$ 
23:    for  $k = 1, \dots, \tilde{K}_l$  do
24:      calculate  $\tilde{K}_l$  intermediate images between  $I_{l,k-1}, I_{l,k}$  with  $v_{l,k}$  using (25)
25:  $\mathbf{I} := \mathbf{I}_0$ 
```

---

## 5. Numerical Examples

In this section, we present numerical examples demonstrating the potential of the method. In the first part, we use the Radon transform as operator. We implemented Algorithm 1 in Matlab. To represent our images on a grid during the registration step we applied the `mex` interface of the spline library by E. Bertolazzi [8] with the Akima splines. To reduce the number of involved parameters in (21), we use  $\lambda = \mu = \nu = 100\eta$  in all our experiments. The remaining parameters  $\alpha, \beta, \lambda$  are optimized with respect to the SSIM via a gridsearch. The parameters in comparison algorithms are SIMM optimized, too. For solving the appearing linear systems of equations in the Quasi-Newton method, we apply a GPU implementation.

In the first part of our experiments, we consider the Radon transform as operator. The second part deals with superresolution, which does not have a continuous counterpart.

## 5.1. Limited Angle and Sparse CT

We are given a reference image  $R \in [0, 1]^{256, 256}$  and sinogram data of a target image  $I_{\text{orig}} \in [0, 1]^{256, 256}$ , which we want to reconstruct. For the numerical implementation of the (discrete) Radon transform, we applied the Astra toolbox [35, 47, 48], which allows more flexibility compared to the built-in Matlab function.

In our **first example**, the reference image consists of 6 triangular shaped objects, which are deformed to stars in the target image, see Fig. 3<sup>1</sup>. The sinogram is obtained by the Radon transform using 10 measurement directions equally distributed (with steps of 9 degrees) from 0 to 81 degrees, i.e. the measurement angle is limited to less than the half domain. The sinogram is additionally corrupted with 5 percent Gaussian noise. We are interested in the reconstruction of the target given the sinogram data. We use a multi grid approach with a down-sampling by a factor of 0.5. For the down-sampling of the sinogram, two neighboring rays are averaged and rescaled to the correct intensity. Note that this is easily possible if the number of rays is chosen appropriately. The result of our TDM-INV algorithm is shown in Fig. 3 (c), where we used the parameters  $\text{lev} = 4$ ,  $\lambda = 0.07$ ,  $\alpha = 0.05$  and  $\beta = 10$ . Compared to the reconstruction by the  $L^2$ -TV model (with  $\lambda_{\text{TV}} = 0.05$ ) in Fig. 3 (d), our method is able to deal with the missing data from 81 to 180 degrees. Visually, the result is almost perfect and also the SSIM value is very good.

The **second example** deals with a more structured image. The given reference image depicts an artificial brain image, and the target can be considered as a deformed version, see Fig. 4<sup>2</sup> and [22]. The sinogram of the target is created using the Radon transform with 20 measurements equally distributed from 0 to 180 degrees and by adding 5 percent Gaussian noise.

The setup is similar to the problem before. The result of TDM-INV shown in Fig. 4 (c) was calculated with the parameters  $\text{lev} = 5$ ,  $\lambda = 0.08$ ,  $\alpha = 0.025$  and  $\beta = 2$ . Since our model can use the reference information as compensation for the sparse data set, our reconstruction is better than those with the  $L^2$ -TV model (with  $\lambda_{\text{TV}} = 0.1$ ) in Fig. 4 (d).

## 5.2. Superresolution

We are given a reference image  $R \in [0, 1]^{256, 256}$  and a low resolution image  $B \in [0, 1]^{64, 64}$  obtained by down-sampling of a target image  $I_{\text{orig}} \in [0, 1]^{256, 256}$  with the down-sampling operator  $P_4 \in \mathbb{R}^{256, 64}$  given by

$$P_4 = \frac{1}{4} \begin{pmatrix} 1 & 1 & 1 & 1 & 0 & & & & & 0 \\ 0 & 0 & 0 & 0 & 1 & 1 & 1 & 1 & 0 & 0 \\ & & & & \ddots & & \ddots & & & \\ 0 & & & & & & & 0 & 1 & 1 & 1 & 1 \end{pmatrix} \in \mathbb{R}^{256, 64}.$$

<sup>1</sup>The images in Fig. 3(a) and (b) are taken from the paper [14] and were provided by Barbara Gris and Ozan Öktem.

<sup>2</sup>available at <http://bigwww.epfl.ch/algorithms/mriphantom/>

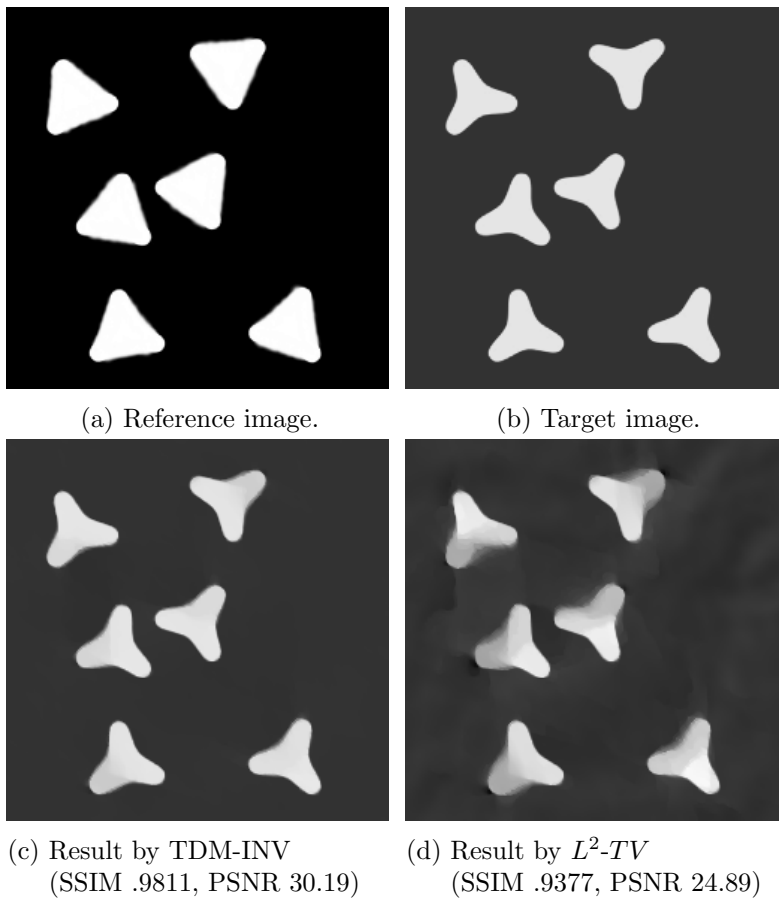


Figure 3: Image reconstruction from sparse, limited angle CT measurements from 0 to 81 degrees with 10 angles.

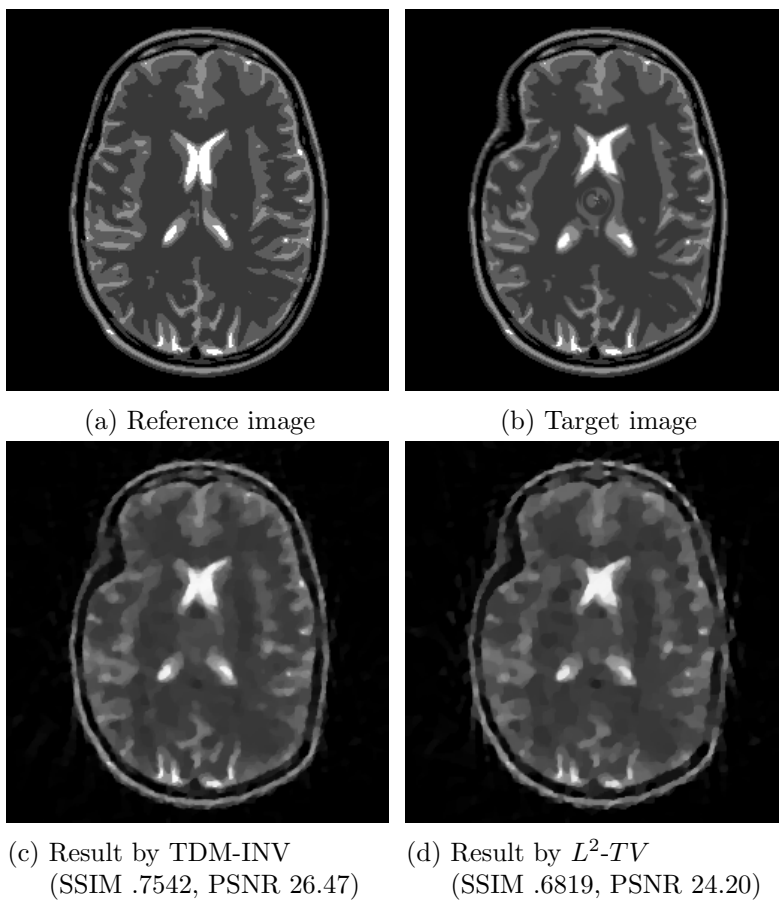


Figure 4: Image reconstruction from sparse CT measurements using 20 angles from 0 to 180 degrees.

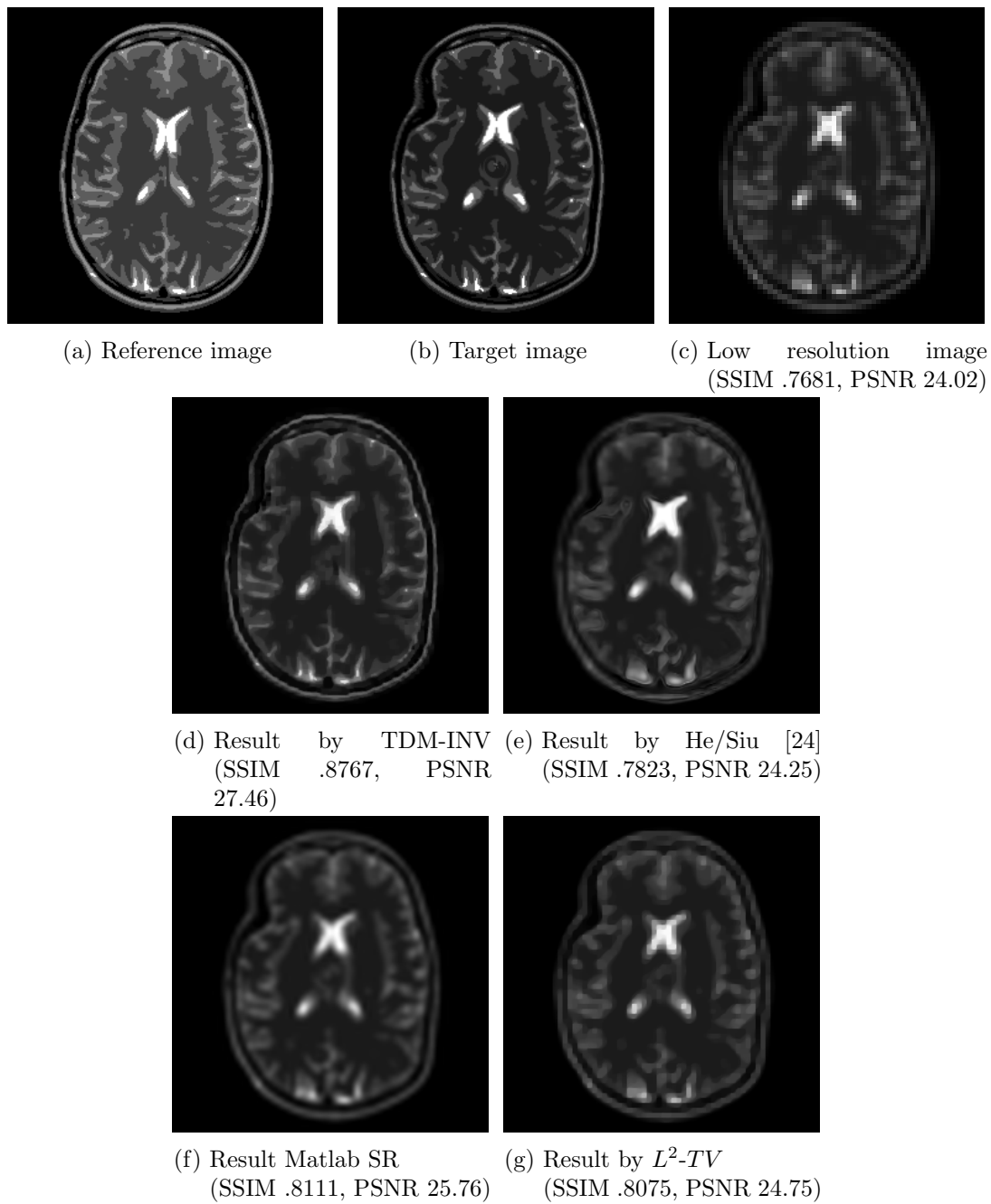


Figure 5: Superresolution from  $64 \times 64$  pixels to  $256 \times 256$  for brain image.

In other words,  $B = P_4 I_{\text{orig}} P_4^T$ . See Fig. 5 (a)-(c). For the multi grid approach we use a downscaling by 50% such that we can use the given image  $B$  for the first three levels, i.e.,  $B_0 = B_1 = B_2 \in \mathbb{R}^{64,64}$ . We adapt the matrix  $P_4 \in \mathbb{R}^{256,64}$  to  $P_2 \in \mathbb{R}^{128,64}$  for the second level and use the identity matrix for all higher levels.

In our **third example** we consider the same reference and target images as in the previous example. The result of TDM-INV is shown in Fig. 5 (d), where used the parameters  $\text{lev} = 4$ , where  $\lambda = 0.01$ , and  $\tilde{K}_3 = 2, \tilde{K}_2 = 0, \tilde{K}_1 = 0, \alpha = 0.001, \beta = 0.5$ . We compare our method with the single image superresolution method of He and Siu [24], which is based on a self-similarity assumption of the high and low resolution image together with a Gaussian process regression. In contrast to the result obtained by this method in cf. Fig. 5 (e), we do not have artifacts around the bright features. Using the Matlab function `imresize`, the best reconstruction is obtained with the “lanczos3” kernel, see Fig. 5 (f), which is affected by a strong blur. For this example, the  $L^2$ -TV (parameter  $\lambda_{\text{TV}} = 0.001$ ) reconstruction yields the result shown in Fig. 5 (g). Comparing all methods, we see that our method is able to recover the fine details as well as the overall structure best.

In our **last example**, we not only deform and scale the given image, but also include a new detail in the image. As mass can be created during the image path, our method is able to reconstruct also the small detail, cf. Fig. 6 <sup>3</sup>, where  $\lambda = 0.01$ , and  $\tilde{K}_3 = 3, \tilde{K}_2 = 1, \tilde{K}_1 = 0, \alpha = 0.001, \beta = 0.5$ . For this simpler image, our method leads to best result in SSIM and PSNR. The result produced by [24] in Fig. 6 (e) yields almost the same SSIM, but visually the method recovers a lot of background noise. The best result of Matlab’s `imresize` is given by the “bilinear” interpolation here. However, this result is affected by a strong blur. The  $L^2$ -TV approach (parameter  $\lambda_{\text{TV}} = 0.001$ ) works better for this simpler image than in the previous example, but is still not able to match our result. Especially the overlapping part in the center of the phantom is only recovered by TDM-INV.

## 6. Conclusions

This paper merges the edge-preserving  $L^2$ -TV variational model for solving inverse image restoration problems with a metamorphosis-inspired approach to utilize information from a reference image. The approach, called TDM-INV, can handle intensity changes between the reference and the image we want to reconstruct. The method gives very good results for artificial images so that we are looking forward to real-world applications in material sciences or medical imaging, e.g. motion models for organs [19, 20]. Several extensions of the model are possible. Due to the finite difference approach more sophisticated regularizers than the TV-term can be simply involved. Another possible modification would be to apply different transport models, see e.g. [26]. Further, the usage of multiple reference image can be taken into account.

---

<sup>3</sup>The images used in Fig. 6 are based on the ones in [21].

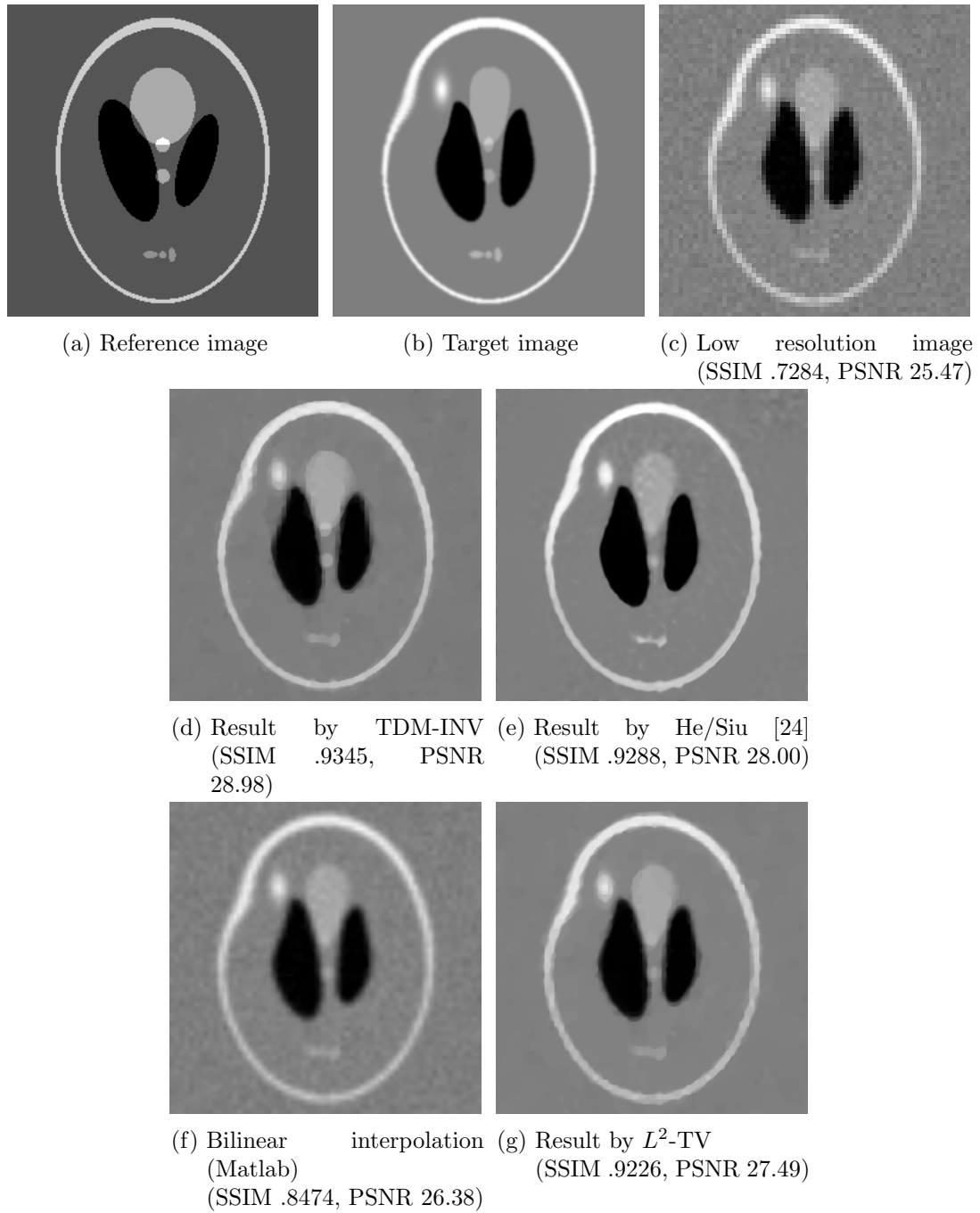


Figure 6: Superresolution from  $64 \times 64$  pixels to  $256 \times 256$  for Shepp-Logan phantom.

## A. Gagliardo-Nirenberg inequality

**Theorem A.0.1** (Gagliardo-Nirenberg [33]). *Let  $\Omega \subset \mathbb{R}^n$  be a bounded domain satisfying the cone property. For  $1 \leq q, r \leq \infty$ , suppose that  $f$  belongs to  $L^q(\Omega)$  and its derivatives of order  $m$  to  $L^r(\Omega)$ . Then for the derivatives  $D^j f$ ,  $0 \leq j < m$  the following inequalities hold true with constants  $C_1, C_2$  independent of  $f$ :*

$$\|D^j f\|_{L^p(\Omega)} \leq C_1 \|D^m f\|_{L^r(\Omega)}^a \|f\|_{L^q(\Omega)}^{1-a} + C_2 \|f\|_{L^q(\Omega)},$$

where  $\frac{1}{p} = \frac{j}{n} + a\left(\frac{1}{r} - \frac{m}{n}\right) + (1-a)\frac{1}{q}$  for all  $a \in [\frac{j}{m}, 1]$ , except for the case  $1 < r < \infty$  and  $m - j - \frac{n}{r}$  is a nonnegative integer, in which the inequality only holds true for  $a \in [\frac{j}{m}, 1)$ .

**Remark A.0.2.** For  $p = q = r = 2$  the inequality simplifies to

$$\begin{aligned} \|D^j f\|_{L^2(\Omega)} &\leq C_1 \|D^m f\|_{L^2(\Omega)}^{\frac{j}{m}} \|f\|_{L^2(\Omega)}^{1-\frac{j}{m}} + C_2 \|f\|_{L^2(\Omega)} \\ &\leq C_1 \|D^m f\|_{L^2(\Omega)} + (C_1 + C_2) \|f\|_{L^2(\Omega)}, \end{aligned}$$

where the second inequality follows by estimating the product by the maximum of both factors.

## Acknowledgments

This work was initialized during an internship of S. Neumayer in the research group of C. Schönlieb in Cambridge. S. Neumayer wants to thank Barbara Gris, Ozan Öktem and Carola-Bibiane Schönlieb for fruitful discussions on the topic. Funding by the German Research Foundation (DFG) within the project STE 571/13-1 and within the Research Training Group 1932, project area P3, is gratefully acknowledged. We gratefully acknowledge the support of NVIDIA Corporation with the donation of the Quadro M5000 GPU used for this research.

## References

- [1] H. W. Alt. *Lineare Funktionalanalysis: Eine anwendungsorientierte Einführung*, volume 6. Springer, Berlin, 2002.
- [2] L. Ambrosio, N. Fusco, and D. Pallara. *Functions of Bounded Variation and Free Discontinuity Problems*. Oxford University Press, 2000.
- [3] J. M. Ball. Global invertibility of Sobolev functions and the interpenetration of matter. *Proceedings of the Royal Society of Edinburgh: Section A Mathematics*, 88(3-4):315–328, 1981.
- [4] A. Beck. *First-Order Methods in Optimization*, volume 25. SIAM, 2017.
- [5] A. Beck and L. Tetruashvili. On the convergence of block coordinate descent type methods. *SIAM Journal on Optimization*, 23(4):2037–2060, 2013.

- [6] M. F. Beg, M. I. Miller, A. Trounev, and L. Younes. Computing large deformation metric mappings via geodesic flows of diffeomorphisms. *International Journal of Computer Vision*, 61(2):139–157, 2005.
- [7] B. Berkels, A. Effland, and M. Rumpf. Time discrete geodesic paths in the space of images. *SIAM Journal on Imaging Sciences*, 8(3):1457–1488, 2015.
- [8] E. Bertolazzi. Splines toolbox. <https://github.com/ebertolazzi/Splines>.
- [9] R. I. Boş and C. Hendrich. A Douglas–Rachford type primal-dual method for solving inclusions with mixtures of composite and parallel-sum type monotone operators. *SIAM Journal on Optimization*, 23(4):2541–2565, 2013.
- [10] K. Bredies and D. Lorenz. *Mathematische Bildverarbeitung*. Vieweg+Teuber, 2011.
- [11] M. Burger, A. Sawatzky, and G. Steidl. First order algorithms in variational image processing. In S. O. R. Glowinski and W. Yin, editors, *Operator Splittings and Alternating Direction Methods, Springer 2017*, 2017.
- [12] A. Chambolle and T. Pock. A first-order primal-dual algorithm for convex problems with applications to imaging. *Journal of Mathematical Imaging and Vision*, 40(1):120–145, 2011.
- [13] A. Chambolle and T. Pock. An introduction to continuous optimization for imaging. *Acta Numerica*, 25:161–319, 2016.
- [14] C. Chen and O. Öktem. Indirect image registration with large diffeomorphic deformations. *SIAM Journal on Imaging Sciences*, 11(1):575–617, 2018.
- [15] G. E. Christensen, R. D. Rabbitt, and M. I. Miller. Deformable templates using large deformation kinematics. *IEEE Transactions on Image Processing*, 5(10):1435–1447, 1996.
- [16] C. De Boor. *A Practical Guide to Splines*, volume 27. Springer-Verlag New York, 1978.
- [17] P. Dupuis, U. Grenander, and M. I. Miller. Variational problems on flows of diffeomorphisms for image matching. *Quarterly of Applied Mathematics*, 56(3):587–600, 1998.
- [18] A. Effland. *Discrete Riemannian Calculus and A Posteriori Error Control on Shape Spaces*. Dissertation, University of Bonn, 2017.
- [19] J. Ehrhardt and C. Lorenz. *4D Modeling and Estimation of Respiratory Motion for Radiation Therapy*. Springer, 2013.
- [20] F. Gigengack, X. Jiang, M. Dawood, and K. P. Schäfers. *Motion Correction in Thoracic Positron Emission Tomography*. Springer, 2015.

- [21] B. Gris, C. Chen, and O. Öktem. Image reconstruction through metamorphosis. *HAL Preprint hal-01773633v1*, Apr. 2018.
- [22] M. Guerquin-Kern, L. Lejeune, K. P. Pruessmann, and M. Unser. Realistic analytical phantoms for parallel magnetic resonance imaging. *IEEE Transactions on Medical Imaging*, 31(3):626–636, 2012.
- [23] E. Haber and J. Modersitzki. A multilevel method for image registration. *SIAM Journal on Scientific Computing*, 27(5):1594–1607, 2006.
- [24] H. He and W.-C. Siu. Single image super-resolution using Gaussian process regression. In *2011 IEEE Conference on Computer Vision and Pattern Recognition (CVPR)*, pages 449–456. IEEE, 2011.
- [25] J. Karlsson and A. Ringh. Generalized Sinkhorn iterations for regularizing inverse problems using optimal mass transport. *SIAM Journal on Imaging Sciences*, 10(4):1935–1962, 2017.
- [26] J. Maas, M. Rumpf, C. Schönlieb, and S. Simon. A generalized model for optimal transport of images including dissipation and density modulation. *ESAIM: Mathematical Modelling and Numerical Analysis*, 49(6):1745–1769, 2015.
- [27] M. I. Miller, A. Trounev, and L. Younes. On the metrics and Euler-Lagrange equations of computational anatomy. *Annual Review of Biomedical Engineering*, 4(1):375–405, 2002.
- [28] M. I. Miller, A. Trounev, and L. Younes. Hamiltonian systems and optimal control in computational anatomy: 100 years since d’arcy thompson. *Annual Review of Biomedical Engineering*, 17:447–509, 2015.
- [29] M. I. Miller and L. Younes. Group actions, homeomorphisms, and matching: A general framework. *International Journal of Computer Vision*, 41(1-2):61–84, 2001.
- [30] J. Modersitzki. *Numerical Methods for Image Registration*. Oxford University Press on Demand, 2004.
- [31] J. Modersitzki. *FAIR: Flexible Algorithms for Image Registration*. SIAM, Philadelphia, 2009.
- [32] S. Neumayer, J. Persch, and G. Steidl. Morphing of manifold-valued images inspired by discrete geodesics in image spaces. *arXiv preprint arXiv:1710.02289*, 2017.
- [33] L. Nirenberg. An extended interpolation inequality. *Annali Della Scuola Normale Superiore di Pisa-Classe di Scienze*, 20(4):733–737, 1966.
- [34] O. Öktem, C. Chen, N. O. Domaniç, P. Ravikumar, and C. Bajaj. Shape-based image reconstruction using linearized deformations. *Inverse Problems*, 33(3):035004, 2017.

- [35] W. Palenstijn, K. Batenburg, and J. Sijbers. Performance improvements for iterative electron tomography reconstruction using graphics processing units (gpus). *Journal of Structural Biology*, 176(2):250–253, 2011.
- [36] J. Persch, F. Pierre, and G. Steidl. Exemplar-based face colorization using image morphing. *Journal of Imaging*, 3(4):Art.Num. 48, 2017.
- [37] T. Pock, A. Chambolle, D. Cremers, and H. Bischof. A convex relaxation approach for computing minimal partitions. *IEEE Conference on Computer Vision and Pattern Recognition*, pages 810–817, 2009.
- [38] L. Rudin, S. Osher, and E. Fatemi. Nonlinear total variation based noise removal algorithms. *Physica D*, 60:259–268, 1992.
- [39] M. Rumpf and B. Wirth. Discrete geodesic calculus in shape space and applications in the space of viscous fluidic objects. *SIAM Journal on Imaging Sciences*, 6(4):2581–2602, 2013.
- [40] M. Rumpf and B. Wirth. Variational time discretization of geodesic calculus. *IMA Journal of Numerical Analysis*, 35(3):1011–1046, 2015.
- [41] O. Scherzer, M. Grasmair, H. Grossauer, M. Haltmeier, and F. Lenzen. *Variational Methods in Imaging*. Springer, 2009.
- [42] H. Schumacher, J. Modersitzki, and B. Fischer. Combined reconstruction and motion correction in spect imaging. *IEEE Transactions on Nuclear Science*, 56(1):73–80, 2009.
- [43] A. Trouvé. An infinite dimensional group approach for physics based models in pattern recognition. *International Journal of Computer Vision*, 1995.
- [44] A. Trouvé. Diffeomorphisms groups and pattern matching in image analysis. *International Journal of Computer Vision*, 28(3):213–221, 1998.
- [45] A. Trouvé and L. Younes. Local geometry of deformable templates. *SIAM Journal of Mathematical Analysis*, 37(2):17–59, 2005.
- [46] A. Trouvé and L. Younes. Metamorphoses through Lie group action. *Foundations in Computational Mathematics*, 5(2):173–198, 2005.
- [47] W. van Aarle, W. J. Palenstijn, J. Cant, E. Janssens, F. Bleichrodt, A. Dabrovolski, J. De Beenhouwer, K. J. Batenburg, and J. Sijbers. Fast and flexible X-ray tomography using the ASTRA toolbox. *Optics Express*, 24(22):25129–25147, 2016.
- [48] W. van Aarle, W. J. Palenstijn, J. De Beenhouwer, T. Altantzis, S. Bals, K. J. Batenburg, and J. Sijbers. The ASTRA toolbox: A platform for advanced algorithm development in electron tomography. *Ultramicroscopy*, 157:35–47, 2015.

- [49] R. L. Wheeden. *Measure and Integral: an Introduction to Real Analysis*, volume 308. CRC Press, 2015.
- [50] L. Younes. *Shapes and Diffeomorphisms*. Springer-Verlag, Berlin, 2010.
- [51] J. Yuan, C. Schnörr, and G. Steidl. Simultaneous higher order optical flow estimation and decomposition. *SIAM Journal of Scientific Computing*, 29(6):2283–2304, 2007.